Technical Note

Institution of MECHANICAL ENGINEERS

Journal of AEROSPACE ENGINEERING

Proc IMechE Part G:
J Aerospace Engineering
2015, Vol. 229(7) 1349–1359
© IMechE 2014
Reprints and permissions:
sagepub.co.uk/journalsPermissions.nav
DOI: 10.1177/0954410014547441
uk.sagepub.com/jaero
SAGE

Behaviour of turbulent Prandtl/Schmidt number in compressible mixing layer

Afroz Javed[1], NKS Rajan[2] and Debasis Chakraborty[1]

Abstract

The behaviour of turbulent Prandtl/Schmidt number is explored through the model-free simulation results. It has been observed that compressibility affects the Reynolds scalar flux vectors. Reduced peak values are also observed for compressible convective Mach number mixing layer as compared with the incompressible convective Mach number counterpart, indicating a reduction in the mixing of enthalpy and species. Pr_t and Sc_t variations also indicate a reduction in mixing. It is observed that unlike the incompressible case, it is difficult to assign a constant value to these numbers due to their continuous variation in space. Modelling of Pr_t and Sc_t would be necessary to cater for this continuous spatial variation. However, the turbulent Lewis number is evaluated to be near unity for the compressible case, making it necessary to model only one of the Pr_t and Sc_t.

Keywords

Compressible mixing layer, turbulent Prandtl/Schmidt number, convective Mach number

Date received: 16 March 2014; accepted: 23 July 2014

Introduction

For all combustion processes, good mixing of fuel and oxidiser is a basic requirement. Owing to the lower pressure conditions combined with low residence time, the mixing process becomes very critical for supersonic combustion ramjet engine applications. The gaseous fuel and oxidiser streams eventually mix along the length of the combustor after injection. In case of the liquid fuels, the atomised fuel droplets evaporate and the gaseous phase mixes and burns along the combustor length. The mixing between the fuel and oxidiser occurs in a mixing layer formed between the two at high compressible speeds. In a study carried out by Jackson and Grosch,[1] it has been reported that the instabilities of the compressible shear flow are predominantly inviscid. In such a scenario, the mixings of mass, momentum and energy are expected to be dominated by turbulent transport as against molecular transport. Thus, the ability to predict turbulent mixing at high compressible speeds is crucial in obtaining accurate numerical simulations for supersonic combustor design and performance evaluation. Computational fluid dynamics (CFD) simulations using Reynolds-averaged Navier–Stokes (RANS) methodology are now routinely used in the scramjet engine development cycle to determine optimal fuel injector arrangements, investigate trends noted during testing and extract various measures of engine efficiency. Massively parallel computing, together with the maturation of CFD codes, has made it possible to perform simulations of complete engine flow paths within a reasonable time using RANS methodology.

In order to model Reynolds stresses arising after the time averaging of Navier–Stokes equations, turbulence models are used in RANS simulations with varying degree of complexity. Similar to Reynolds stress in Navier–Stokes equation, Reynolds heat flux vectors arise in time-averaged energy equation and Reynolds mass flux vectors in time-averaged species equations. The turbulent transport of a scalar property has historically been modelled using the gradient diffusion hypothesis. This model choice assumes that the turbulent transport of the scalar is in the direction

[1]Directorate of Computational Dynamics, Defence Research and Development Laboratory, Kanchanbagh, Hyderabad, India
[2]Department of Aerospace Engineering, Indian Institute of Science, Bangalore, India

Corresponding author:
Debasis Chakraborty, Directorate of Computational Dynamics, Defence Research and Development Laboratory, Kanchanbagh P.O., Hyderabad 500058, India.
Email: debasis_cfd@drdl.drdo.in

Downloaded from pig.sagepub.com at DEFENCE RESEARCH DEV LAB on June 11, 2015

of decreasing values for that scalar. This leads to the following expression for the Reynolds heat flux and mass flux vectors.

$$\overline{\rho h'' u''_j} = -\frac{\mu_t}{Pr_t}\frac{\partial \tilde{h}}{\partial x_j} \tag{1}$$

$$\overline{\rho Y''_n u''_j} = -\frac{\mu_t}{Sc_t}\frac{\partial \tilde{Y}_n}{\partial x_j} \tag{2}$$

The diffusion rates are controlled by specifying the turbulent Prandtl (Pr_t) and Schmidt (Sc_t) numbers. The turbulent Prandtl number specifies the ratio of the rate of turbulent momentum transport to rate of turbulent energy transport, while the turbulent Schmidt number defines the ratio of the turbulent momentum transport rate to turbulent mass transport rate.

It has been indicated by experimental measurements and direct numerical simulation (DNS) studies that Pr_t and Sc_t numbers for averaged flow fields can vary significantly in different regions of the flow even for relatively simple shear flows like boundary layers, jets and wakes.[2–5] A review on the turbulent Prandtl/Schmidt number in several free shear flows made by Reynolds[3] gives following variations (from core to outer region): round jet 0.73–1.7; round wake 0.8–0.3; plane jet 0.5–1.3; plane wake 0.5–0.7. In another review made by Baurle[5] for high-speed reacting flows, the range of turbulent Prandtl number variations for planar jets from 0.2 to 3.0, for round Jets 0.7 to 2.0 and for backward facing step from 0.7 to 3.0. In the same review, the variation of the turbulent Schmidt number is found for planer jets from 0.1 to 2.2, for round jets from 0.1 to 2.0, for jet into cross-flow from 0.1 to 0.5, and for injection behind a bluff body it is from 0.2 to 0.7. The variations observed in the values of Pr_t and Sc_t in these reviews indicate that these numbers are dependent on the type of flow as well as the spatial region in the flow. However, it has been general practice to assume a constant value of Pr_t and Sc_t in RANS computations. Choice of a unique value of these parameters for a simulation of a complex flow, especially in the case where no information is available about the turbulent Prandtl/Schmidt number variations can lead to incorrect predictions. Several computations[6–9] performed by different authors have at times shown an extreme sensitivity to values assumed for these parameters. For example, in the study carried out by Baurle and Eklund[7] for a scramjet combustor at Mach 4.0 flight condition, a variation of turbulent Schmidt number from 0.25 to 0.75 resulted in unstart of the intake due to intense heat release at lower turbulent Schmidt number and unsustained combustion due to low turbulent mass transfer at higher turbulent Schmidt number. At lower values of turbulent Prandtl number, the increased turbulent thermal diffusion process allowed heat to be transferred away from the flame-holding (recirculation) zones at a rate that was not sustainable causing flame blow-out. Due to this kind of sensitivity of Scramjet performance parameters on the choice of values for turbulent Prandtl/Schmidt number, it would be tempting to look for a direct solution of the Reynolds heat and mass flux vectors transport equations with suitable modelling for unclose terms. However, even if suitable models were available to close each of the scalar flux equations, the number of additional equations introduced would greatly exceed the number of equations required to solve the continuity and momentum equations with suitable modelling. Clearly, it would be impractical to include a full second-order closure model in simulations of engineering interests. To address this problem, many studies have been carried out by coupling the gradient diffusion hypothesis with models that allow the turbulent Prandtl and/or Schmidt number to vary spatially.

Several authors[10–13] have pursued the development of models that allow for spatial variation of turbulent Prandtl Schmidt numbers within the context of gradient diffusion hypothesis. These models involve additional transport equation for the scalar variance and its dissipation rate. Xiao et al.[11] have compared some of the available experimental data for scramjet combustors, using their two-dimensional (2D) simulation model for variable turbulent Prandtl and Schmidt numbers, and satisfactory matches are shown. Xiao et al.[14] have also validated variable Schmidt number formulation for Scramjet applications through 2D simulations. Keistler et al.[15] have used models for the prediction of turbulent Prandtl/Schmidt numbers for simulations of supersonic combustors from two different experiments (SCHOLAR and HyShot). Comparisons were made with available measurements of pressure temperature and composition, and fair to good agreement was observed. However, many authors have also shown that combustor flows could be modelled with a constant value of turbulent Prandtl and Schmidt number. Jiang and Campbell[16] have shown through their 2D/axisymmetric simulations with the available experimental results that an average value of $Pr_t = Sc_t = 0.7$ could be used for the numerical simulations. Also it is found that lower values have also been used by different authors to get satisfactory results. $Pr_t = Sc_t = 0.2$ was used by He et al.[17] for mixing of a gaseous jet in air cross-flow, and by Kaaling et al.[18] for their studies on a low-emission combustor design. Both these studies showed good match with the available experimental data. Star et al.[19] performed simulations for HyShot supersonic combustor experiments with different turbulent Prandtl/Schmidt numbers combinations. It was observed that the best pressure match with

Downloaded from pig.sagepub.com at DEFENCE RESEARCH DEV LAB on June 11, 2015

experimental data for pressure was obtained with a constant value of $Sc_t = 0.5$ and $Pr_t = 0.7$.

Although the use of variable turbulent Prandtl/Schmidt number formulation does not require a priori knowledge of suitable values of these numbers, the constant turbulent Prandtl/Schmidt number methodology is computationally simple. Owing to the kind of sensitivity of the performance parameters of Scramjet engine on turbulent Prandtl/Schmidt numbers, it is essential to know the behaviour of these numbers in a high-speed compressible mixing layer. The information about the variation of these numbers within a compressible mixing layer allows one to choose from variable or constant turbulent Prandtl/Schmidt number formulations. In large eddy simulations (LES) also, turbulent Prandtl and Schmidt numbers are important parameters as they occur in subgrid models. It has been shown by Ingenito and Bruno,[20] in their numerical simulations for a supersonic combustor that variation of Sc_t can give completely different flow structures.

Javed et al.[21] simulated the high-speed confined mixing layer experimental case of Erdos et al.[22] through model-free simulation. In the simulation, mixing of two high-speed streams of Hydrogen and Nitrogen of convective Mach number (M_c) of 0.82 at different temperatures, velocity and density are considered. Here, the convective Mach number, M_c, is defined as $\Delta U/(a_1 + a_2)$, with ΔU as the velocity difference between the two mixing streams and a_1 and a_2 are the speeds of sound in the two streams. The model-free simulation data have been analysed to explore the behaviour of turbulent Prandtl number and turbulent Schmidt number profiles at these high-compressible speeds. Separate simulations are also carried out for low convective Mach number of 0.1, and the profiles of turbulent Prandtl and Schmidt numbers are compared between the two cases.

Numerical simulation of the mixing layer

A DNS can resolve the full range of physical scales of motion without need of any turbulence model, but its application is limited to flows with a relatively small Reynolds numbers. Whereas RANS simulations require an eddy viscosity which must be adjusted to correlate with experiments and is thus not always robust. Higher Reynolds numbers are possible with LES, whose basic idea is to apply spatial filter(s) at a length scale Δ and include a subgrid model for the filtered stress terms, e.g. Smagorinsky model, to relegate the empiricism to just the smallest scales (although dynamic subgrid modelling shows promise in removing this as well). LES is increasing being used in the development of scramjet engine. But these hi-fidelity methods remain as analysis tools mainly because of severe computational requirement and geometrical complexities. As Δ is decreased for a flow problem of given length scale, the subgrid model contribution is reduced and accuracy is increased. For some very high Reynolds number turbulent flows, if Δ is sufficiently reduced but is still greater than the Kolmogorov scale, the subgrid model influence becomes approximately negligible *if the flow is not controlled by a laminar sublayer*. Such flows include high Reynolds number turbulent free shear layers, jets, wakes and some sharp corner separated flow regimes for which further increases in Reynolds number do not significantly influence the bulk of the mean and turbulent field. Therefore, for a particular class of flows for which sufficient resolution is applied, one may simply neglect the filtering and the subgrid model stress terms and therefore eliminate any adjustable coefficients other than cell resolution. An extensive review of the model-free simulation method and results for both non-reacting and reacting flows is provided by Givi.[23] This methodology of model-free simulations has been used by many researchers and reported in literature. High-resolution non-linear inviscid simulations were performed by Oh and Loth[24] for M_c values of 0.35, 0.45 and 0.7. The growth rate reduction with increasing M_c is well captured, the profiles of velocity, and turbulence intensities match satisfactorily with the experimental observations of Goebel and Dutton.[25] Oh and Loth[24] carried out the study of the mixing layers in a 2D domain, 400 mm long and 47.6 mm wide to match experimental test set up size of Goebel and Dutton.[25] Euler equations were solved using the argument that viscous effect does not play a dominant role in the mixing layer region. The finest grid consisted of 20,000 points with a minimum grid spacing of 0.3 mm. Also, it was reported that in order to achieve a good grid convergence the value of $\Delta x_{min}/b$ should be equal to or lesser than 0.05 (for a second-order numerical scheme[26]), where b is local shear layer thickness and Δx_{min} is the grid resolution. In another study involving the use of model-free simulations, Risha[27,28] considered a three-dimensional domain of size 100 mm × 10 mm × 17 mm and used a grid size of $100 \times 53 \times 35$ for studying free mixing layers formed between two air streams at different convective Mach numbers ($M_c = 0.2$–1.56) and obliquity angles. The model-free simulations carried out by Chakraborty et al.[29] shows a good match of the wall pressures for the mixing study of the confined compressible mixing layer. The grid independence of the solution was demonstrated by not only comparing the mean values of the various thermochemical profiles with different grids but also higher order quantities. A good prediction of the different flow quantities in the compressible regime, by model-free simulation technique makes it a suitable choice for the present study.

Hydrogen and Nitrogen at Mach numbers of 3.09 and 3.99 respectively flow in the upper and lower parts of a rectangular duct, forming a mixing layer.

Downloaded from pig.sagepub.com at DEFENCE RESEARCH DEV LAB on June 11, 2015

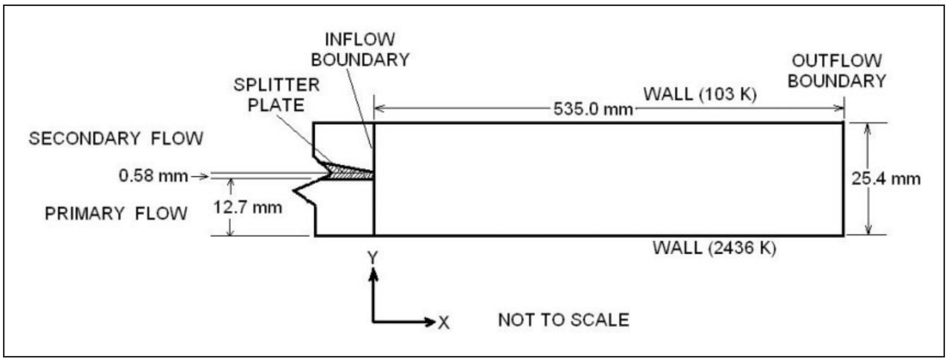

Figure 1. Schematic of experimental condition of Erdos et al. for confined supersonic mixing layer.

Table 1. Inflow parameters for non-reacting shear layer of experimental condition of Erdos et al.[22]

Location	Species	Velocity (m/s)	Temperature (K)	Pressure (Pa)	Mach number	Re/mm
Primary	Nitrogen	3807	2436	27580	3.99	2200
Secondary	Hydrogen	2389	103	27580	3.09	42000

Table 2. Inflow parameters for non-reacting shear layer corresponding $M_c = 0.1$.

Location	Species	Velocity (m/s)	Temperature (K)	Pressure (Pa)	Mach number	Re/mm
Primary	Nitrogen	1409	2436	27580	1.4	814
Secondary	Hydrogen	1231	103	27580	1.6	21600

A schematic of the experiment along with the flow parameters is shown in Figure 1. The cross-section after the splitter plate is 25.4 mm high and 50.8 mm wide, and the details of the inflow parameters are presented in Table 1.

To compare the behaviour of Pr_t and Sc_t with an incompressible convective Mach number case ($M_c = 0.1$) with the inflow parameters shown in Table 2 is also studied. In this case, both the streams maintain same pressure, temperature, composition and density as in Erdos' experimental case. The only difference is the velocities of the streams are reduced while keeping the individuals Mach numbers supersonic. Also, the Reynolds numbers of the streams are reduced in proportion to the reduction in the speed of the streams.

Computational methods

Compact finite difference scheme – Method, grid and boundary conditions

2D model-free simulations are carried out by employing non-reacting version of SPARK2D code developed at the NASA LaRC by Drummond[30] and Carpenter.[31] It discretises 2D Navier–Stokes equations by using Mac-Cormack's compact scheme with fourth-order spatial and second-order temporal accuracy. This choice represents a compromise between the accuracy of higher order numerical algorithm and the robustness and efficiency of low-order methods. This code has been validated by comparing the computed results of some test problems with known analytical solutions. Carpenter and Kamath[32] have demonstrated that with the compact scheme, the growth rate with the initial profile based on the eigen functions predict those from linear stability theory for free shear layer to within 1% for a time duration equal to about five times the sweep time of the flow field. The compact scheme provide a substantial reduction in truncation and phase errors over the first-order upwind and the second-order Mac-Cormack's scheme.

The flow domain is of size 535 mm $\times$ 25.4 mm. The two streams are separated by a splitter plate at a height of 12.7 mm, before the start of mixing. The grid is stretched exponentially in the axial direction with minimum grid spacing at the inflow boundary to capture the initial development of the mixing layer. In the lateral direction, minimum grid spacing is taken near the interface, and it is stretched exponentially towards both the upper and lower wall. The wall boundary layer is resolved by taking very fine mesh near the solid wall, and the grid is again stretched exponentially in the region away from the wall. The grid structure employed in the simulations

Downloaded from pig.sagepub.com at DEFENCE RESEARCH DEV LAB on June 11, 2015

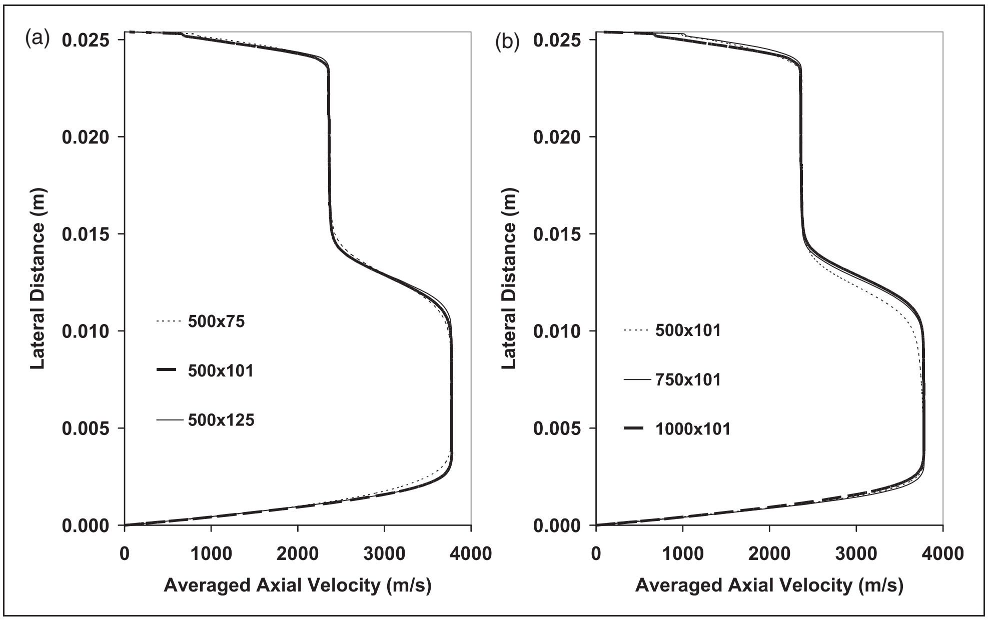

Figure 2. Averaged axial velocity variation in lateral direction at an axial location of 300 mm obtained with grid refinement in (a) lateral direction and (b) axial direction.

has 1000 points in the axial direction with minimum grid size of 0.3 mm near the inflow boundary plane and the maximum size of 0.8 mm near the outflow boundary. In the lateral direction, 101 grid points are employed with minimum grid spacing of 0.09 mm near the interface and wall and the maximum grid spacing is of the order of 0.5 mm in the region away from interface and wall. The grid considered in the simulation is sufficient to capture the large-scale structure of the flow field as is evident from the grid resolution studies. Grid resolution calculations were made by varying the number of grids in both the axial and lateral directions. In this grid resolution study, five different grids namely, 1000×101, 750×101, 500×101, 500×125 and 500×75 were used to determine the effect of grid resolution in the axial and cross-stream directions. Initially, one sweep time for the flow is assumed as the time taken for the flow to cross the domain with lower velocity stream. The results for first two such sweep times are discarded, and the variables are averaged for next two sweeps. The value of averaged axial velocity at a plane 300 mm from the inlet is shown in Figure 2(a) and (b) for both lateral and axial refinement of the grids. It can be observed that increasing the number of grids from 500 to 1000 in axial direction and 75 to 125 in the lateral direction leaves the results almost unchanged. The spectral content of pressure fluctuations was compared with different grid and is observed that not only the mean values but also the amplitudes of the fluctuations match well with different grid. Hence, it is concluded that the 1000×100 grid is sufficient to give grid-independent solution.

The boundary conditions set for this problem are as follows. In the solid boundary at the upper and lower walls, no slip conditions for the velocities and the constancy of wall temperatures are imposed. A boundary layer velocity profile is given at the inlet as shown in Figure 3. Both the streams are given equal pressure of 27580 Pa. Nitrogen mass fraction is set to unity for primary stream, while Hydrogen mass fraction is unity for the secondary stream. The static temperatures of both primary and secondary streams are set at constant values of 2436 K and 103 K, respectively. The exit boundary condition is obtained by second-order extrapolation and is considered satisfactory for this problem dominated by supersonic flow.

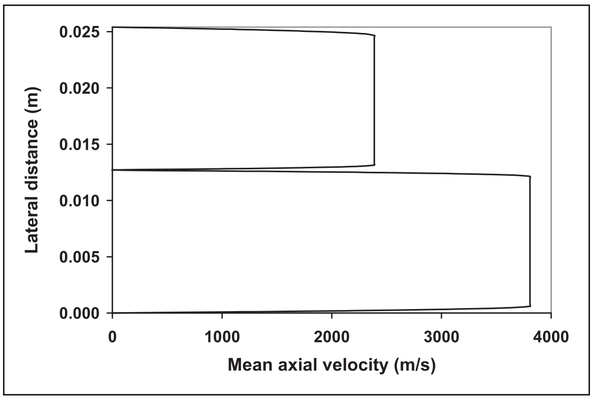

Figure 3. Axial mean velocity profile at the inlet (edge of splitter plate).

The mean properties of the flow can be calculated after the initial conditions have been purged out of the flow domain. The fluid speed inside the domain varies from zero at the walls to the speed of the high-speed stream. In this situation, it is difficult to assign a

Downloaded from pig.sagepub.com at DEFENCE RESEARCH DEV LAB on June 11, 2015

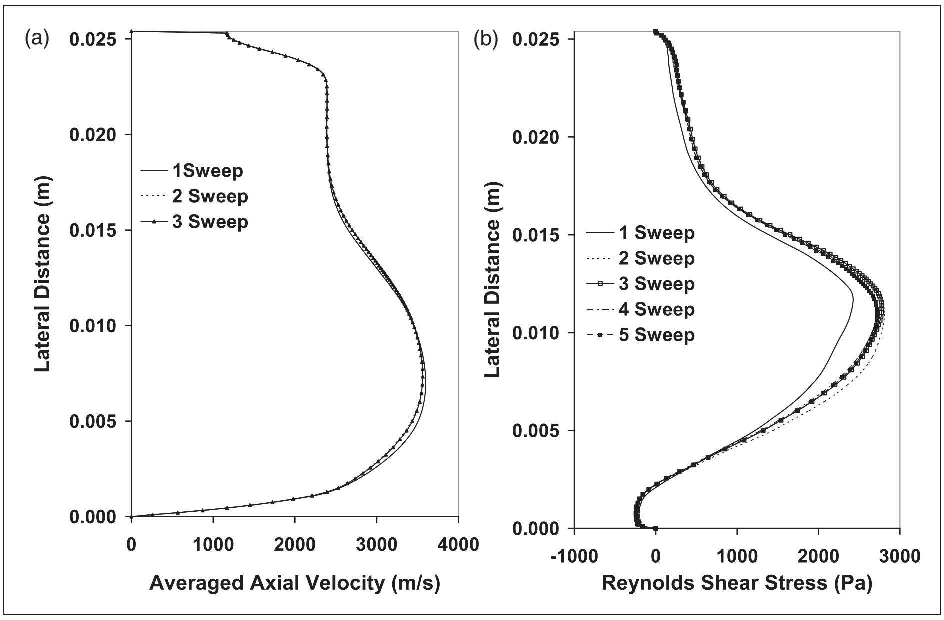

Figure 4. Variation of the averaged variables with sweep times in the lateral direction at an axial location of 500 mm: (a) axial velocity and (b) Reynolds shear stress.

characteristic speed which could be indicative of purging time. In order to evaluate the time needed to purge out the initial conditions, a third chemical species is added in the initial condition, and its concentration is monitored. Similar method has been adopted to check the purging of initial conditions by Lian et.al.[33] for their unsteady simulation of a combustor. The initial condition for the species is given as mass fraction of 0.5 of an inert species in the entire flow domain to serve as a 'marker' for ascertaining the purging of initial conditions. The monitoring of this inert species shows that it takes 515 µs for its maximum mass fraction to become less than 1×10^{-6} within the entire flow domain. Changing the initial conditions with different velocities also does not change this purge time. The averaging process for the evaluation of mean quantities is started after this purging time of 515 µs.

The attainment of statistical steady state is checked by averaging the values of the required variables over time, after the purging of initial conditions. Different flow variables are averaged as the solution proceeds, and these values are checked at different intervals for stabilised values. The time interval chosen for checking the stabilisation of averaged quantities is taken same as that taken for purging the initial condition, i.e. 515 µs. This time interval is referred as one sweep time for the purpose of checking the attainment of statistical steady state. It has been observed that the mean properties like velocities, temperature and species mass fractions stabilise at less number of sweeps than the turbulence statistics quantities like Reynolds stress and Reynolds fluxes. It was found that all the mean and turbulent quantities reach their statistical steady state after four sweeps of run. The variation of averaged axial velocity and Reynolds stress in lateral direction at an axial location of 500 mm, with number of sweeps are shown in Figure 4. The final average values of the variables are taken by averaging the instantaneous values for time taken for four sweeps that is 2060 µs.

Same grid is considered for incompressible convective Mach number case, and similar procedure is carried out for evaluation of purging time followed by averaging of the variables four sweeps time.

For the evaluation of the turbulent Prandtl and Schmidt number, the values of turbulent viscosity and turbulent scalar fluxes are required. The isotropic turbulent viscosity coefficient is used in the closure for the Reynolds stress tensor, generally used in the linear models based on the Boussinesq approximation, as given below

$$\overline{\rho u''_i u''_j} = -\mu_t\left(\frac{\partial \tilde{u}_i}{\partial \tilde{x}_j} + \frac{\partial \tilde{u}_j}{\partial \tilde{x}_i}\right) + \frac{2}{3}\delta_{ij}\left(\bar{\rho}k + \mu_t\frac{\partial \tilde{u}_k}{\partial \tilde{x}_k}\right) \tag{3}$$

where μ_t is isotropic eddy viscosity coefficient. In a mixing layer, the mixing of axial momentum in the lateral direction is of utmost importance. Thus, the turbulent viscosity coefficient could be evaluated as the following

$$\mu_t = \frac{\overline{\rho u'' v''}}{\left(\frac{\partial \tilde{u}}{\partial y} + \frac{\partial \tilde{v}}{\partial x}\right)} \tag{4}$$

Using gradient transport hypothesis, a turbulent heat transfer coefficient can be defined as

$$\alpha_t = \frac{\overline{\rho h'' v''}}{\left(\frac{\partial \tilde{h}}{\partial y}\right)} \tag{5}$$

Downloaded from pig.sagepub.com at DEFENCE RESEARCH DEV LAB on June 11, 2015

Similarly, turbulent mass transfer coefficient is expressed as

$$D_t = \frac{\overline{\rho Y''_{H2} v''}}{\left(\frac{\partial \tilde{Y}_{H2}}{\partial y}\right)} \tag{6}$$

The values of the Reynolds heat flux and Reynolds mass flux are evaluated by averaging the data of the simulations. The averaged values are evaluated as

$$\overline{\rho u'' v''} = \overline{\rho u v} - \bar{\rho}\tilde{u}\tilde{v} \tag{7}$$

$$\overline{\rho h'' v''} = \overline{\rho h v} - \bar{\rho}\tilde{h}\tilde{v} \tag{8}$$

$$\overline{\rho Y''_{H2} v''} = \overline{\rho Y_{H2} v} - \bar{\rho}\tilde{Y}_{H2}\tilde{v} \tag{9}$$

The first terms on right-hand sides of equations (7) to (9) are evaluated as follows

$$\overline{\rho u v} = \frac{\sum_{ti}^{tf} \rho u v \Delta t}{\sum_{ti}^{tf} \Delta t} \tag{10}$$

where ti is the initial time for averaging, tf is the final time, and Δt is the time step. In the similar manner, the first terms on the right-hand side of equations (8) and (9) are also evaluated. The average density is evaluated as

$$\bar{\rho} = \frac{\sum_{ti}^{tf} \rho \Delta t}{\sum_{ti}^{tf} \Delta t} \tag{11}$$

The Favre-averaged values are evaluated as

$$\tilde{u} = \frac{\sum_{ti}^{tf} \rho u \Delta t}{\sum_{ti}^{tf} \rho \Delta t} \tag{12}$$

Similarly, Favre-averaged values of v, h and Y_{H2} are also evaluated. While evaluating the values in this fashion, the variables are not required to be saved in a separate file as a time series, and thus any number of sweeps could be averaged without the problem of storage space.

Finally, the values of turbulent Prandtl and Schmidt numbers are evaluated as follows

$$Pr_t = \frac{\mu_t}{\alpha_t} \tag{13}$$

and

$$Sc_t = \frac{\mu_t}{D_t} \tag{14}$$

The turbulent Lewis number is defined as

$$Le_t = \frac{Sc_t}{Pr_t} \tag{15}$$

Results and discussions

For both the Erdos' experimental case and incompressible convective Mach number case, the average enthalpy and species profiles collapse in a self similar like profiles. These profiles are plotted against a normalised lateral distance, defined as, $\eta = (y - y_c)/\delta_\xi$. y_c is the lateral distance where $(\xi - \xi_2)/(\xi_1 - \xi_2) = 0.5$, and δ_ξ is the thickness of the mixing layer defined as the distance between the transverse locations where $(\xi - \xi_2)/(\xi_1 - \xi_2)$ is 0.99 and 0.01. In case of the enthalpy profiles, ξ is replaced with h, and for Hydrogen mass fraction profiles, it is replaced with Y_{H2}. In case of average axial velocities, ξ is replaced with u, for the calculation of y_c. However, the definition of thickness does not work by simply replacing ξ by u. As the flow proceeds downstream due to presence of weak oblique shock waves and viscous effects the free stream velocities decrease for both the streams, and within a short distance the thickness parameter $(u–u_2)/(u_1–u_2)$ does not reach a value of 0.99 in the high-speed stream and reaches a value of 0.01 before the end of mixing layer in the low-speed stream. In order to get around this problem, another measure of mixing layer thickness namely vorticity thickness defined as $\delta_\omega = \Delta U/(\frac{\partial u}{\partial y})_{\max}$ is used which is shown to have almost same value as defined by 1% definition for free shear layers. Figure 5 shows these profiles for both the convective Mach number cases.

For the incompressible convective Mach number case, it is observed in Figure 5(a) that all the three similarity profiles within the mixing layer show kind of collapse with almost equal slopes. While for higher convective Mach number, as shown in Figure 5(b), the normalised enthalpy profiles shows a slightly increased value within mixing layer due to more viscous heating arising from higher velocities of the flow.

The Reynolds heat and mass fluxes are normalised with $\rho_{ave}\Delta U$, where ρ_{ave} is the average density of the two streams. The values of normalised turbulent scalar fluxes are shown in Figure 6. The peak values are seen to be higher for the incompressible convective Mach number case. However, the difference between the peak values are not as high as observed by Freund et al.[34] for DNS simulation of an annular jet, and also that observed by Ribault[35] for the simulation of a plane compressible mixing layer. In both these numerical studies, the Reynolds number is kept almost constant for incompressible and compressible convective Mach number simulations. However, in the present study, the Reynolds number is around 50% lower for incompressible case. This lower Reynolds number could be a reason for this low difference in the peak values of the Reynolds scalar flux vectors.

The turbulent Prandtl and Schmidt numbers are evaluated and plotted in Figure 7. Both turbulent Prandtl and Schmidt number for incompressible convective Mach number case show a fairly constant

Downloaded from pig.sagepub.com at DEFENCE RESEARCH DEV LAB on June 11, 2015

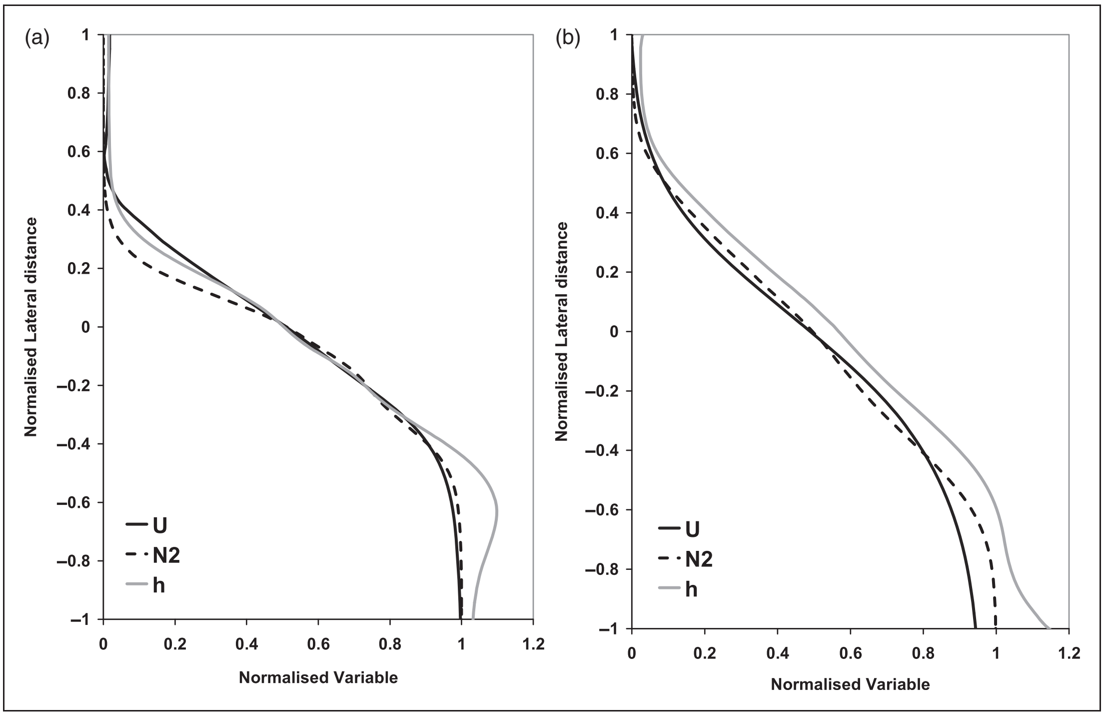

Figure 5. Similarity profiles for normalised scalar values and average axial velocities for (a) $Mc = 0.1$ and (b) $Mc = 0.8$.

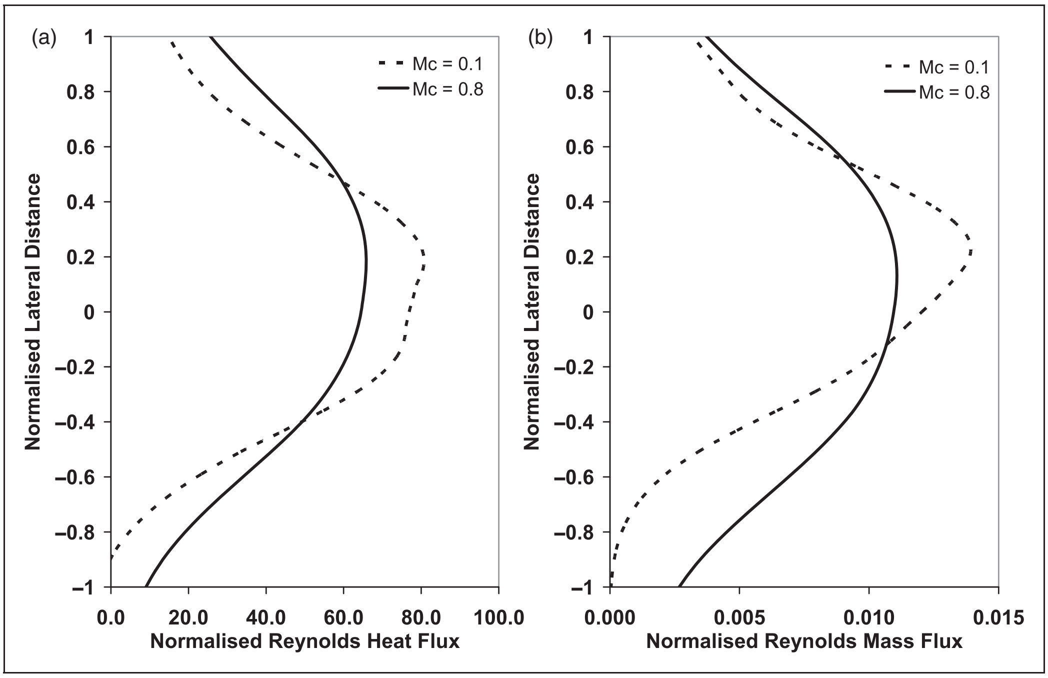

Figure 6. Normalised values of (a) Reynolds heat flux and (b) Reynolds mass flux.

value within the mixing layer region. The turbulent Prandtl number for the incompressible case is close to 0.5, the value suggested for shear layers by Wilcox.[36] It is evident that specification of constant turbulent Prandtl/Schmidt number works with a good degree of accuracy for incompressible, to weakly compressible flows. However, for highly compressible flows like Erdos' experimental case, a continuous variation in turbulent Prandtl/Schmidt number can be observed from Figure 7. This continuous variation in the values of these numbers makes it difficult to choose a constant value for a particular problem. Assigning a constant value may result in a completely different situation than that expected.

Downloaded from pig.sagepub.com at DEFENCE RESEARCH DEV LAB on June 11, 2015

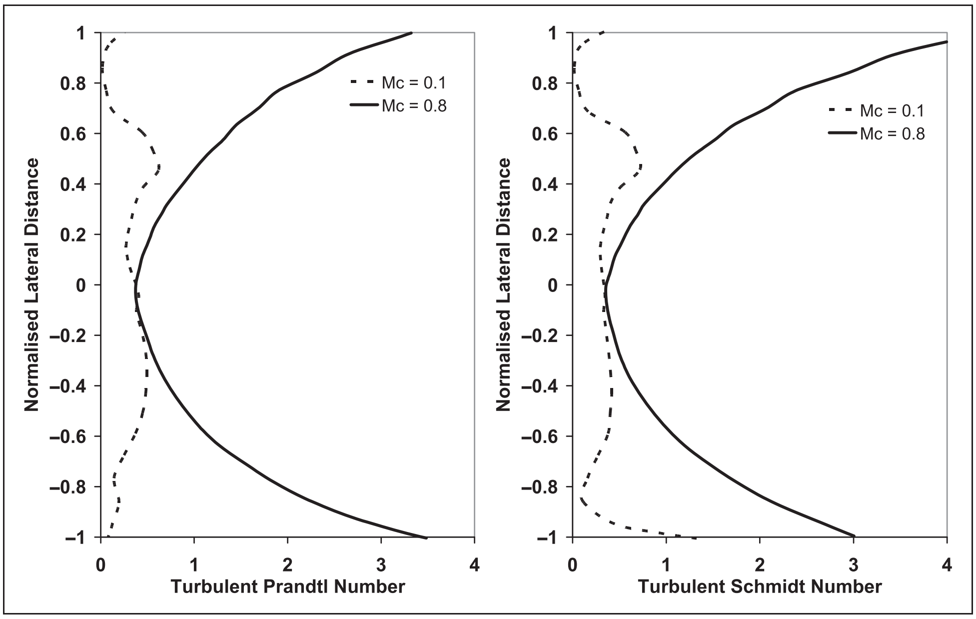

Figure 7. Turbulent Prandtl and Schmidt numbers variations.

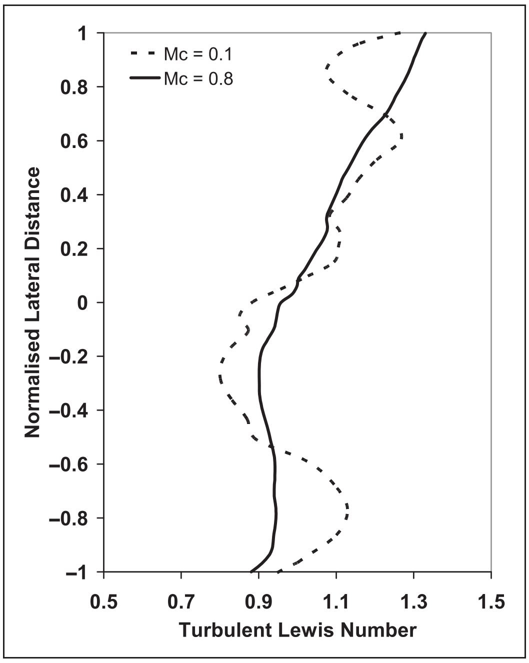

Figure 8. Turbulent Lewis number variation.

The turbulent Lewis number is shown in Figure 8. It can be observed that it does not vary very significantly from unity for both high and low convective Mach number cases. For high convective Mach number case, the turbulent Lewis number remains near unity in the Nitrogen side of the flow and then shows an increasing trend indicating a dominance of turbulent heat transfer over turbulent mass transfer. This near-unity value for compressible non-reacting case indicates that only one of the numbers from Pr_t and Sc_t needs to be modelled for such cases as suggested by Xiao et al.[11] also.

Conclusions

A numerical study has been carried out using model-free simulations to get an understanding of behaviour of Pr_t and Sc_t in a compressible mixing layer. Two cases have been simulated, one with the Erdos' experimental condition and the other with an incompressible convective Mach number. The Reynolds heat flux and Reynolds mass flux show reduction in peak values for compressible convective Mach number. The values of turbulent Prandtl and turbulent Schmidt numbers indicate that for an incompressible convective Mach number, assignment of a constant value to these numbers may give fairly accurate results. However, the variation observed within the mixing layer for these numbers in case of compressible mixing layers suggests that prescription of a constant value may not be a good idea. And for accurate modelling of mixing in a compressible mixing layer, modelling of these numbers would be a requirement. However, the near-unity value of turbulent Lewis number observed for this case indicates that modelling of only one of these two numbers (Pr_t and Sc_t) would be sufficient.

Funding

This research received no specific grant from any funding agency in the public, commercial, or not-for-profit sectors

Conflict of interest

None declared.

References

1. Jackson TL and Grosch CE. *Absolute/convective instabilities and the convective Mach number in a compressible mixing layer*. ICASE Report No. 181861, June 1989.

Downloaded from pig.sagepub.com at DEFENCE RESEARCH DEV LAB on June 11, 2015

2. Launder BE. Heat and mass transport. In: Bradshaw P (ed.) *Turbulence*. Vol. 12 of Topics in applied physics. Berlin Heidelberg: Springer, 1976, pp.232–287.
3. Reynolds AJ. The variation of turbulent Prandtl and Schmidt numbers in wakes and jets. *Int J Heat Mass Trans* 1976; 19: 757–764.
4. Kays WM. Turbulent Prandtl Number – Where are we? *ASME J Heat Trans* 1994; 116: 284–295.
5. Baurle RA. *Modelling of high speed reacting flows: established practices and future challenges*. AIAA paper No. 2004-0267, 2004.
6. Baurle RA, Alexopoulos GA and Hassan HA. Analysis of supersonic combustors with swept ramp injectors. *J Propul Power* 1997; 3: 327–328.
7. Baurle RA and Eklund DR. Analysis of dual mode hydrocarbon scramjet operation at Mach 4-6.5. *J Propul Power* 2002; 18: 990–1002.
8. Riggins DW, Mao M, Bittner RD, et al. *Numerical modelling of normal fuel injection: effect of turbulent Schmidt number*. NASP report, Ref. WBS 2.4.09, 1989.
9. Eklund DR, Baurle RA and Gruber MR. *Computational study of a supersonic combustor fuelled by an aerodynamic ramp injector*. AIAA Paper 2001-0379, 2001.
10. Nagano Y and Kim C. A two – equation model for heat transport in wall turbulent shear flows. *J Heat Trans* 1988; 110: 583–589.
11. Xiao X, Hassan HA and Baurle RA. *Modelling scramjet flows with variable turbulent Prandtl and Schmidt numbers*. AIAA Paper No. 2006-128, 2006.
12. Reynolds AJ. The prediction of turbulent Prandtl and Schmidt numbers. *Int J Heat Mass Trans* 1975; 18: 1055–1069.
13. Chidambaram N, Dash SM and Kenzakowski DC. *Scalar variance transport in the turbulence modeling of propulsive jets*. AIAA paper 99-0235, 1999.
14. Xiao X, Edwards JR, Hassan HA, et al. Variable Schmidt number formulation for scramjet application. *AIAA J* 2006; 44: 593–599.
15. Keistler PG, Hassan HA and Xiao X. Simulation of supersonic combustion in three-dimensional configurations. *J Propul Power* 2009; 25: 1233–1239.
16. Jiang LY and Campbell I. Prandtl/Schmidt number effect on temperature distribution in a generic combustor. *Int J Therm Sci* 2009; 48: 322–330.
17. He G, Guo Y and Hsu AT. The effect of Schmidt number on turbulent scalar mixing in a jet-in-crossing flow. *Int J Heat Mass Trans* 1999; 42: 3727–3738.
18. Kaaling H, Ryden R, Bouchie Y, et al. *RQL combustor development including design, CFD calculations, CARS measurements and combustion tests*. ISABE 97-7069, 1997.
19. Star JB, Edwards JR, Smart MK, et al. *Investigation of scramjet flow path instability in a shock tunnel*. AIAA paper No. 2006-3040, 2006.
20. Ingenito A and Bruno C. *LES of a supersonic combustor with variable turbulent Prandtl and Schmidt numbers*. AIAA Paper No. 2008-515, 2008.
21. Javed A, Paul PJ and Chakraborty D. Model free simulations for compressible mixing layer. *J Aerosp Eng* 2013; 227: 977–991.
22. Erdos J, Tamagno J, Bakos R, et al. *Experiments on shear layer mixing at hypervelocity conditions*. AIAA Paper 92-0628, 1992.
23. Givi P. Model free simulations of turbulent reactive flows. *Prog Energy Combust Sci* 1989; 15: l–107.
24. Oh CK and Loth E. *A numerical investigation of supersonic turbulent shear layers: compressibility effects*. AIAA Paper No. 94-2244, 1994.
25. Goebel SG and Dutton JC. *Velocity measurement of compressible, turbulent mixing layers*. AIAA paper 90-0709, 1990.
26. Oh CK and Loth E. Effects of initial conditions on spatially evolving compressible shear layer simulations. *Comput Fluid Dyn* 1996; 6: 307–319.
27. Risha DJ. *Analysis of growth rates in three-dimensional air-to-air, supersonic shear layers using direct numerical simulation*. AIAA paper No. 95-0523, 1995.
28. Risha DJ. *Analysis of turbulence statistics in three-dimensional, air-to-air supersonic shear layers using direct numerical simulation*. AIAA paper No. 95-6072, 1995.
29. Chakraborty D, Mukunda HS and Paul PJ. Two dimensional direct numerical simulation of nonreacting confined supersonic mixing layer. *Aeronaut J* 2000; June: 291–296.
30. Drummond JP. Supersonic reacting internal flow field, in numerical approaches in combustion modeling. In: Oran ES and Borris JP (eds) *Progress in aeronautics and astronautics*, 1991, AIAA, 135: 365–420.
31. Carpenter MH. *A generalized chemistry version of SPARK*. NASA-CR-4196, 1998.
32. Carpenter MH and Kamath H. *Three dimensional extension to the SPARK combustion code NASA-Langley*, 1988, NASA-CP-5029: 107–137.
33. Lian C, Merkle CL and Xia G. Flowfield initialisation and approach to stationary conditions in unsteady combustion simulations. *Comput Fluids* 2010; 39: 310–323.
34. Freund JB, Moin P and Lele SK. Compressibility effects in a turbulent annular mixing layer. Part 2. Mixing of a passive scalar. *J Fluid Mech* 2000; 421: 269–292.
35. Ribault CL. Large eddy simulation of passive scalar in compressible mixing layers. *Int J Heat Mass Trans* 2008; 51: 3514–3524.
36. Wilcox DC. *Turbulence modeling for CFD*. La Canada: DCW Industries Inc, 1994, p.182.

Appendix

Notations

D_t	turbulent mass transfer coefficient
h	enthalpy
k	turbulent kinetic energy
t	time
u	axial component of velocity
v	lateral component of velocity
x	axial distance
y	lateral distance
Y	species mass fraction

Downloaded from pig.sagepub.com at DEFENCE RESEARCH DEV LAB on June 11, 2015

α_t	turbulent heat transfer coefficient	$\sim$	Favre-averaged value
μ_t	eddy viscosity	$''$	fluctuating component from Favre averaging
ρ	density		

Superscripts

—	Reynolds-averaged value

Downloaded from pig.sagepub.com at DEFENCE RESEARCH DEV LAB on June 11, 2015